

1 **Atlas-based data integration for mapping the connections and**
2 **architecture of the brain**

3

4

5 Trygve B. Leergaard & Jan G. Bjaalie

6

7 Neural Systems Laboratory, Institute of Basic Medical Sciences, University of Oslo,

8 Norway

9

10 Corresponding author. E-mail: t.b.leergaard@medisin.uio.no

11

12

13 Detailed knowledge about the neural connections among regions of the brain is key
14 for advancing our understanding of normal brain function and changes that occur
15 under ageing and disease. Researchers employ a range of experimental techniques to
16 map connections at different levels of granularity in rodent animal models, but the
17 results are often challenging to compare and integrate. Three-dimensional reference
18 atlases of the brain provide new opportunities for cumulating, integrating, and
19 reinterpreting research findings across studies. We review approaches for integrating
20 data describing neural connections and other modalities in rodent brain atlases and
21 discuss how atlas-based workflows can facilitate brain-wide analyses of neural
22 network organization in relation to other facets of neuroarchitecture.
23
24

25 **Introduction**

26 The brain is composed of vast numbers of neurons, glia, and vasculature, encased
27 within a solid skull. It processes and stores information, generates memories, thoughts
28 and ideas, performs planning, and effectuates a wide range of behaviours. Dendrites
29 and axons allow neurons to transmit signals across shorter or longer distances, and
30 axons profusely branch into terminal fields with multiple synaptic contacts to other
31 neurons. The functions performed by neurons are to a high degree determined by their
32 connections with other neurons within and across brain regions.

33 Large ensembles of widely distributed neurons make up complex neural
34 networks. The networks are highly organized, typically with different cell types
35 distributed in layers or clusters. Within the network, populations of neurons exert
36 specific excitatory, inhibitory or modulatory influences on other parts of the network,
37 and variations in the strengths and spatial distributions of the connections, including
38 specific patterns of divergence and converge, influence how the network subserves its
39 functions. Overall, knowledge about the organization of the networks – the wiring
40 patterns of the brain – is critical for understanding normal brain function, and is
41 typically embedded in network models aimed at elucidating and studying a variety of
42 brain functions (1). Insight into the detailed organization of wiring patterns is also key
43 to understanding and treating brain disorders. One example is the use of knowledge
44 about the wiring of deep brain structures (Fig. 1AB) for treatment of neurological
45 disease, e.g., the use of electrical stimulation targeting the subthalamic nucleus or
46 specific parts of the thalamus for ameliorating symptoms of Parkinson’s disease and
47 medication-resistant tremor (2).

48 While the patterns of neural wiring direct how neural signals are distributed
49 through a network, the functional characteristics of a network also depend on the
50 physiological and neurochemical properties of neurons, their detailed local cellular
51 relationships to other neurons (micro-circuitry) and to supporting cells with sustaining
52 or modulatory functions. Comprehensive knowledge about how the brain exerts its
53 functions thus requires integration of knowledge about all these features. We argue
54 that recently introduced three-dimensional (3D) digital brain atlases (3-6) offer new
55 opportunities for extensive data integration aimed at improving our understanding of
56 the organization of the brain. These integration efforts are accelerated by the use of
57 tools for registration of heterogeneous data types to the atlases, in combination with
58 computerized workflows for subsequent automated analyses of large data collections.

59 Focusing on the rodent brain as a model system for basic neuroscience, we review
60 approaches for the mapping of neural connections and atlas-based solutions for
61 integrating and analysing data, before discussing future directions for advancing the
62 field.

63

64 **Mapping brain connections**

65 A variety of techniques are available for mapping of neural connections at different
66 levels of granularity. The overall trajectories of fibre bundles in the brain can be
67 visualized with myelin staining (e.g. 7, 8; Fig. 2B) or polarized light imaging in
68 histological sections (e.g. 9; Fig. 2B), and whole brain diffusion MRI methods (e.g. 8,
69 10, 11; Fig. 2B). The “neuron-by-neuron” connections are mapped with use of high-
70 resolution microscopic techniques allowing imaging of tracer-filled individual
71 neurons (e.g. 12, 13), or by use of serial electron microscopy visualization of cellular
72 and synapse ultrastructure (e.g. 14). The current foundation for whole- brain mapping
73 of neuronal connections is, however, provided by invasive tract-tracing experiments
74 in wild-type and transgenic animals (Figs. 1, 2; 15, 16). These methods are highly
75 suitable for describing connections at the level of groups of neurons, demonstrating
76 patterns that are persistent and reproducible among individuals and useful for
77 inferring functional properties and disease related changes (for a discussion of
78 different levels of connectivity analysis, see, 17).

79 In classical tract-tracing experiments, a tracer substance is deposited in a
80 specific location in the brain and taken up by groups of neurons (Fig. 1C-E). The
81 tracer is transported along the axons of the neurons, either anterogradely from
82 neuronal cell bodies to their axonal terminal fields, or retrogradely from axonal
83 terminal fields to the neurons of origin, or in both directions (15, 16). Depending on
84 the tracer employed, some of the morphologies of the labelled neurons are revealed,
85 or the tracer is transported across synapses, allowing identification of pre- and
86 postsynaptic connections in a network (16). New genetic animal constructs have also
87 opened for advanced cell-type specific tracing paradigms, with genetically controlled
88 expression of signals (18).

89 A key methodological innovation for the tract-tracing methods has been serial
90 two-photon tomography (19). By allowing block-face acquisition of high-resolution
91 microscopic images, this technology has been successfully utilized by the Allen
92 Institute to generate large volumes of microscopic 3D tract-tracing image data

93 showing brain wide connections in the mouse brain (5, 18). Using a similar approach,
94 the MouseLight project of Janelia Research Campus has created high-resolution
95 volumetric reconstructions of individual axonal trajectories across entire mouse brains
96 (20, 21).

97

98 **Atlases for brain-wide mapping of connections and related features**

99 Traditionally, experimental tract tracing studies have focussed on one or a few brain
100 regions at a time, yielding precise information about the connections among a few
101 selected regions of interest. Extensive literature mining efforts have aggregated
102 information from available publications into databases, to attain a more complete
103 understanding of the connections between brain regions (22, 23). However, these
104 valuable resources are limited by the diversity of the methods used, the variable levels
105 of precision in the reporting of brain location, and the lack of access to the underlying
106 data (17, 24). Regarding reporting of the anatomical location of observations, a recent
107 analysis of practices and precision from 120 different rodent brain experimental
108 studies revealed substantial differences in the research design, interpretation of
109 results, and reproducibility among reports (25). The main challenges were related to
110 the use of different parcellation schemes and the lack of precision in the reporting of
111 how observations would map onto a given anatomical scheme. While atlases for
112 mouse and rat brains (26-28) have assisted researchers for decades in assigning
113 location to their observations, their utility is limited in that they are two-dimensional
114 and lack efficient and standardized tools for the registration of observations to the
115 atlases. These limitations have been overcome with a new generation of open access
116 3D atlases, which integrate information from multiple anatomical parcellation
117 schemes and have powerful tools for the registration of data to atlases and atlas based
118 analysis.

119 For the mouse brain, the atlases developed by the Allen Institute for Brain
120 Science have become widely used resources. The most recent version is defined in a
121 high-resolution image volume constructed by interpolation of serial two-photon
122 tomography (STPT) images from 1675 adult mice (the Allen Mouse Brain Common
123 Coordinate Framework, CCFv3). In this population-averaged image volume many
124 anatomical delineations were defined using information from a large body of
125 multimodal image data registered to the CCFv3 template (6). The underlying images
126 included the collection of STPT data created for the Allen mouse brain connectivity

127 atlas (5). Additional images were readily integrated into the atlas volume using the
128 same high-throughput imaging and informatics pipeline, as achieved with the
129 inclusion of more than 1,000 STPT image volumes from tract-tracing experiments
130 conducted in transgenic Cre-dependent mice (17).

131 For the rat brain, the Waxholm Space (WHS) atlas is now available in a
132 version 4 with brain-wide parcellation (RRID: SCR_017124; <https://nitrc.org>). This
133 atlas is based on a single high-resolution *ex vivo* structural and diffusion magnetic
134 resonance imaging volume, in which brain regions have been identified and
135 delineated by manual interpretation of the underlying MRI data, enriched with
136 multiple microscopic image data showing different facets of the neuroarchitecture (4,
137 29, 30; see also, Fig. 2). The atlas has seen broad interest as reflected in close to
138 25,000 downloads, more than 300 citations, and inclusion in several services or
139 products (e.g., EBRAINS research infrastructure, <https://ebrains.eu>, and the Neuroinfo
140 software of MBF Bioscience). To facilitate comparisons of different atlas parcellation
141 schemes, seven versions of the Paxinos and Watson rat brain atlases, and four
142 versions of the Swanson rat brain atlas, were registered to the WHS rat brain atlas (31,
143 32).

144

145 **Atlas-based data integration and analysis**

146 The 3D reference atlas spaces provided by the Allen Mouse Brain Common
147 Coordinate Framework (CCFv3 and earlier versions), and the WHS rat brain atlas are
148 useful frameworks for integrating heterogeneous data originating from different
149 researchers and research projects. Recently introduced tools and workflows designed
150 for use with the mouse and rat atlases support a 3-step process for data integration and
151 analysis (Fig. 3): 1) registration of images to atlas, 2) sharing of registered images
152 with viewing and navigation of images in atlas space, 3) extraction of features from
153 the images followed by quantification of the distribution of features within and across
154 brain structures. Below, we review the principles and practical implementation of the
155 three steps, taking a starting point in the EBRAINS Atlases services
156 (<https://ebrains.eu/services/atlasses>) for the mouse and rat brain and the EBRAINS
157 Data and Knowledge services for data sharing and access
158 (<https://ebrains.eu/services/data-and-knowledge>).

159

160

161 *Registration of images to atlas*

162 Data integration requires that the data are made comparable, as if data of different
163 origin were part of a single data set. Thus, the registration of data of different origin to
164 the same atlas framework is a key step towards integration. In EBRAINS, series of 2D
165 histological images of mouse or rat brains are spatially registered to the atlases by an
166 initial landmark-based anchoring of sections, followed by a non-linear adjustment.
167 The EBRAINS tools supporting this step are the QuickNII tool for affine registration
168 (RRID: SCR_016854; 33), and the VisuAlign tool for non-linear registration
169 adjustments (RRID: SCR_017978). The output of the registration process is referred
170 to as *spatial metadata*: a set of anchoring vectors and deformation fields that together
171 define the transformations between the image data and the atlas. A range of other
172 registration tools are available, with some having been developed for particular use
173 cases such as analysing electrode tracts (34, 35), and others suitable for many data
174 modalities (36).

175

176 *Sharing, viewing, and navigating images in atlas space*

177 In addition to having spatial metadata, data are integrable only if they are properly
178 annotated with metadata and other structured information that help us understand the
179 data. Furthermore, the data will have to be discoverable and accessible. The approach
180 taken by the EBRAINS Share data service (<https://ebrains.eu/service/share-data>) is to
181 provide procedures for annotation of the data with metadata according to a metadata
182 standard, and to provide descriptions and other information required to make the data
183 interpretable and reusable. Following a curation of the metadata, the data are stored in
184 the EBRAINS data repository, whereas the metadata are ingested in a knowledge
185 graph which makes the data findable through a Search user interface
186 (<https://search.kg.ebrains.eu>), or a programmatic access route
187 (<https://ebrains.eu/service/find-data/>). A search points the user to Data cards with
188 information about the data, access to the data sets, and also links to a virtual
189 microscopy viewer for inspection of the image data integrated in the atlas.

190 With use of the EBRAINS tools, a broad range of data generated with
191 different methods and in different animals have been registered to the atlases. Figure 2
192 shows examples of histological images registered to the WHS rat brain atlas v4. In the
193 thalamus, as the selected region of interest, data on specific connections of the
194 primary somatosensory cortex are available together with images showing bundles of

195 axons and their orientation with myelin staining and polarized light imaging. Figure
196 2C demonstrates some of the basic functionalities of the virtual microscopy viewer
197 that is available via the Data cards. The viewer supports web-based pan-and-zoom of
198 high-resolution images with overlays of the atlas parcellation map generated by a
199 volumetric atlas slicer. The user can inspect the images at cellular resolution and
200 observe brain regions, names, and boundaries and annotate points of interest to extract
201 atlas coordinates.

202

203 *Feature extraction, quantification, and distribution*

204 Finally, features from the images can be extracted, sorted by brain region, and
205 displayed and further analysed in 3D. To this end, various approaches are employed
206 as exemplified in the EBRAINS workflow for automation of several of the steps (37,
207 38). This workflow consists of a registration tool, a machine learning based tool for
208 extraction of selected features in the images (Ilastik, 39), and finally a tool for
209 quantifying the features per atlas region (Nutil, 38). The workflow allows the users to
210 customise their analysis in many aspects, including choosing the granularity level of
211 the atlas, defining their own regions of interest, filtering artefacts, and applying
212 quality control steps. It also allows export of coordinates to other tools for 3D
213 visualization of the distribution of the selected features, from the whole brain or
214 selected regions. Figure 4 shows examples of regional analysis of brain connection
215 features extracted from images registered to the WHS rat brain atlas and the Allen
216 Mouse Brain Common Coordinate Framework.

217 Figure 4 shows examples of regional analyses of brain connection features
218 extracted from images registered to the WHS rat brain atlas or the Allen Mouse Brain
219 Common Coordinate Framework. The data originate from different research projects
220 and data repositories, but are integrated and made comparable by registration to the
221 same atlas spaces. Specific combinations of tract-tracing data showing terminal fields
222 of axons in the corticopontine projection system have been selected for analysis of
223 topographical organization (Fig. 4A-D), and identification of changes in topography
224 resulting from lack of specific gene expression (Fig. 4E,F). Furthermore, tract-tracing
225 data showing corticopontine projections from large groups of cortical neurons have
226 been combined with 3-D reconstructions showing individual neurons and their
227 extensive branching patterns, including branching to multiple target clusters within

228 the pontine nuclei and elsewhere in the brain stem (Fig. 4G, H), illustrating
229 opportunities for parallel processing and neural circuit complexity.

230

231 **Conclusion and outlook**

232 Online repositories containing large collections of experimental data integrated in an
233 open access volumetric reference atlas have proven successful for mouse brain
234 research, evident from the impressive data and results provided, e.g., by the Allen
235 Institute and the Janelia Research Campus (5, 18, 20, 21). Open access sharing of
236 standardized data mapped in an appropriate anatomical context make it possible to
237 find and efficiently use new combinations of data, suitable for characterizing and
238 investigating many aspects of brain connections. However, despite the impressive
239 amounts of data presented, attempts to utilize these generous resources may also
240 reveal that data coverage may be insufficient to answer challenging questions, as
241 exemplified in the recent study by Tocco et al. (40), demonstrating that studies of
242 topographic organization in the corticopontine projection require precisely
243 corresponding tracer injections to detect subtle changes occurring in transgenic
244 animals (Fig. 4E,F). Similarly, attempts to compare the individual axonal
245 morphologies in the pontine nuclei (using data from the MouseLight project at Janelia
246 Research Campus) to the terminal fields visualized in tract-tracing experiments (using
247 data from the Allen Mouse Brain Connectivity Atlas) reveal that data mapped to the
248 same atlas allow interesting observations (Fig 4G,H), but also indicate that more data
249 are needed for complete mapping of neural networks. Attempts to find, visualize, and
250 compare such data are also hampered by technical challenges related to lack of tools
251 interoperability. In the rat, large data collections on neural connections are not
252 available, and so far few attempts have been made to systematically map brain-wide
253 connections (24). For these reasons, adding more data and tools will be critical for
254 attaining an increasingly complete overview of the organization of brain connections
255 and other features of rodent brain architecture.

256 The atlases play a key role in this endeavour. They provide a standardized
257 representation of anatomical location and are embedded in software tools for
258 integration and analysis. Data sharing services, such as delivered by EBRAINS,
259 organize the data, and help standardize the metadata, including metadata about the
260 location of research data from the brain. Through the atlas frameworks, data from
261 individual researchers published in research articles and integrated in the atlases are

262 made directly comparable to data from large scale mapping efforts such as the Allen
263 Mouse Brain Connectivity Atlas, and the MouseLight project. The new paradigm for
264 research on brain connections and brain architecture in general is to bring the research
265 data into the same reference space, share the data, and prepare the data for systematic
266 reanalysis and reinterpretations of our understanding of the brain. With these new
267 approaches being introduced in neuroscience, literature mining can be supplemented
268 with powerful mining of the data underlying the interpretations included in
269 publications.

270

271 **Acknowledgements**

272 We thank the current and past members of the Neural Systems Laboratory for their
273 contributions to the development, application, and validation of new methods to
274 experimental research in small animal models, and colleagues in the EBRAINS
275 research infrastructure for their contributions to the delivery of services. **Funding:**
276 This work was in part supported by the European Union's Horizon 2020 Framework
277 Program for Research and Innovation under the Specific Grant Agreement No.
278 945539 (Human Brain Project SGA3), and The Research Council of Norway under
279 Grant Agreement No. 269774 (INCF Norwegian Node). **Contributions:** The authors
280 conceived and wrote the paper together. **Competing interests:** The authors state no
281 competing interests. **Advisory affiliations:** JGB is a member of the Management
282 Board of the EBRAINS AISBL, Brussels, Belgium. **Data and code availability:**
283 Data and code used in the present report are publically available as stated for each
284 data collection or software tool.

285

286

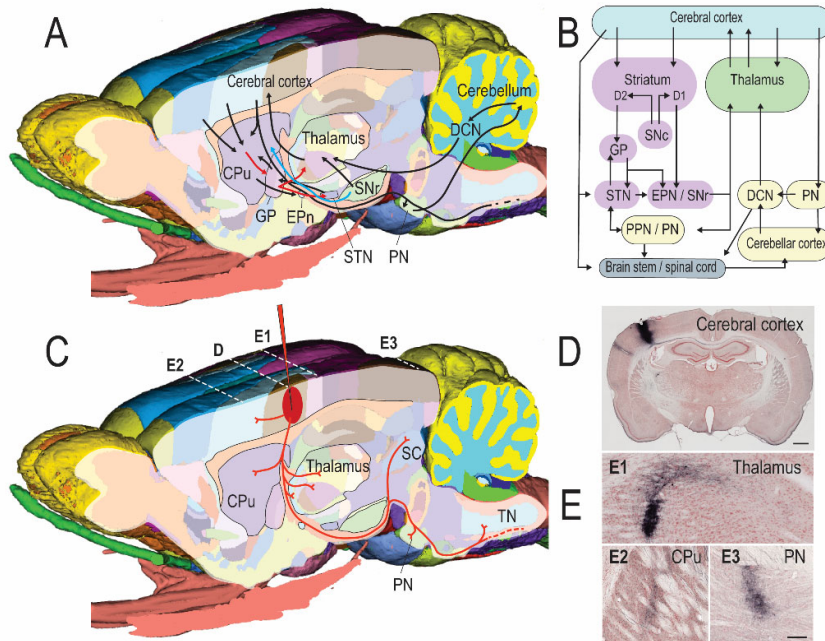
287 **References and Notes**

- 288 1. O. Sporns, *Nat. Neurosci.* **17**, 652-660 (2014).
- 289 2. T. Wichmann, M.R. DeLong, *Neurotherapeutics*.**13**, 264 (2016).
- 290 3. K. Amunts et al., *Science*. **340**, 1472 (2013).
- 291 4. E. A. Papp, T. B. Leergaard, E. Calabrese, G. A. Johnson, J. G. Bjaalie,
292 *NeuroImage*. **97**, 374 (2014).
- 293 5. S. W. Oh et al., *Nature*. **508**, 207 (2014).
- 294 6. Q. Wang et al., *Cell*. **181**, 936 (2020).

- 295 7. T. B. Leergaard et al., *PloS one*. **5**, e8595 (2010).
- 296 8. N.S. White, T. B. Leergaard, H. D'Arceuil, J. G. Bjaalie, A. M. Dale, *Hum. Brain*
297 *Mapp.* **34**, 327 (2013).
- 298 9. N. Schubert, M. Axer, U. Pietrzyk, K. Amunts, in *High-resolution Neuroimaging*,
299 ed. A.M. Halefoglou (Intechopen) (2017).
- 300 10. S. Mori, P. C. van Zijl, *NMR Biomed.* **15**, 468 (2002).
- 301 11. B. Jeurissen, M. Descoteaux, S. Mori, A. Leemans, *NMR Biomed.* **32**, e3785
302 (2019).
- 303 12. R. Parekh, G.A. Ascoli, *Neuroscientist* **21**, 241-254 (2015).
- 304 13. M. Wang et al., *Nature Comm.* **13**, 13:1531, 2022.
- 305 14. N. Turner et al., *Cell* **185**, 1082-1100 (2022).
- 306 15. J. L. Lanciego, F. G. Wouterlood, *J. Chem. Neuroanat.* **42**, 157-183 (2011).
- 307 16. J. L. Lanciego, F. G. Wouterlood, *Brain Struct. Funct.* **225**, 1193 (2020).
- 308 17. J. W. Bohland et al., *PLoS Comput. Biol.* **5**, (2009).
- 309 18. J. A. Harris et al., *Nature*. **575**, 195 (2019).
- 310 19. T. Ragan et al., *Nat. Methods* **9**, 255-256 (2012).
- 311 20. M. N. Economo, J. Winnubst, E. Bas, T. A. Ferreira, J. Chandrasekar, *J. Comp.*
312 *Neurol.* **527**, 2190-2199 (2019).
- 313 21. J. Winnubst et al., *Cell* **179**, 268-281 (2019).
- 314 22. M. Bota, S. Talpalaru, H. Hintiryan, H. W. Dong, L. W. Swanson, *J. Comp.*
315 *Neurol.* **522**, 3160 (2014).
- 316 23. N. M. van Strien, N. L. Cappaert, M. P. Witter, *Nat. Rev. Neurosci.* **10**, 272
317 (2009).
- 318 24. I.M. Zakiewicz, Y. C. van Dongen, T. B. Leergaard, J. G. Bjaalie, *PLoS One*. **6**,
319 e22669 (2011).
- 320 25. I. E. Bjerke et al., *Front. Neuroanat.* **12**, 82 (2018).
- 321 26. G. Paxinos, C. Watson, The rat brain in stereotaxic coordinates. Academic Press,
322 Waltham (1982).
- 323 27. L.W. Swanson, Brain maps: Structure of the rat brain. Amsterdam: Elsevier
324 (1992).
- 325 28. K.B. Franklin, G. Paxinos, The mouse brain in stereotaxic coordinates. Academic
326 Press, Waltham (1996).
- 327 29. L. J. Kjonigsen, S. Lillehaug, J. G. Bjaalie, M. P. Witter, T. B. Leergaard,
328 *NeuroImage*, **108**, 441 (2015).

- 329 30. K.K. Osen, J. Imad, A. E. Wennberg, E. A. Papp, T. B. Leergaard, *NeuroImage*.
330 **199**, 38 (2019).
- 331 31. I. E. Bjerke, U. Schlegel, M. A. Puchades, J. G. Bjaalie, T. B. Leergaard, Human
332 Brain Project Neuroinformatics Platform (2019). [https://doi.org/10.25493/APWV-](https://doi.org/10.25493/APWV-37H)
333 [37H](https://doi.org/10.25493/APWV-37H).
- 334 32. I. E. Bjerke, U. Schlegel, M. A. Puchades, J. G. Bjaalie, T. B. Leergaard, Human
335 Brain Project Neuroinformatics Platform. (2019). [https://doi.org/10.25493/486N-](https://doi.org/10.25493/486N-966)
336 [966](https://doi.org/10.25493/486N-966)
- 337 33. M.A. Puchades, G. Csucs, D. Ledergerber, T. B. Leergaard, J. G. Bjaalie, *PLoS*
338 *One*. **14**, 5 (2019).
- 339 34. P. Shamash, M. Carandini, K. Harris, N. Steinmetz, *bioRxiv*
340 <https://doi.org/10.1101/447995> (2018).
- 341 35. J. Paglia, P. Saldanha, J. G. Fuglstad, J. R. Whitlock, *bioRxiv*
342 <https://doi.org/10.1101/2021.10.01.462770> (2021).
- 343 36. D. Fürth et al., *Nat. Neurosci.* **21**, 139-149 (2018).
- 344 37. S.C. Yates et al., *Front Neuroinform.* 3;13:75. (2019).
- 345 38. N. Groeneboom, S.C. Yates, M.A. Puchades, J.G. Bjaalie, Nutil: *Front*
346 *Neuroinform.* **14**:37 (2020).
- 347 39. S. Berg et al., *Nat. Methods* **16**, 1226-1232 (2019)
- 348 40. C. Tocco, M. Øvsthus, J. G. Bjaalie, T. B. Leergaard, M. Studer, *Development*
349 **149**, dev200026 (2022).
- 350 41. I. M. Zakiewicz, Y. Van Dongen, T.B. Leergaard, J.G. Bjaalie. (2019). Human
351 Brain Project Neuroinformatics Platform. <https://doi.org/10.25493/9MNV-Y97>
- 352 42. I. M. Zakiewicz, Y. Van Dongen, T.B. Leergaard, J.G. Bjaalie. (2019). Human
353 Brain Project Neuroinformatics Platform. <https://doi.org/10.25493/ZF26-DZK>
- 354 43. T. B. Leergaard, S. Lillehaug, A. Dale, J. G. Bjaalie. (2018). Human Brain Project
355 Neuroinformatics Platform. <https://doi.org/10.25493/C63A-FEY>
- 356 44. N. Schubert et al. (2019). Human Brain Project Neuroinformatics Platform.
357 <https://doi.org/10.25493/F9RX-65U>
- 358 45. T.B. Leergaard et al. (2020). EBRAINS. <https://doi.org/10.25493/XQ7V-QN9>
- 359 46. T.B. Leergaard, K.D. Alloway, J.J. Mutic, J.G. Bjaalie, J. G. (2020). EBRAINS.
360 <https://doi.org/10.25493/NECX-22S>
- 361 47. T.B. Leergaard et al. (2020). EBRAINS. <https://doi.org/10.25493/1SSX-606>

- 362 48. T.B. Leergaard, J.G. Bjaalie (2020). EBRAINS. <https://doi.org/10.25493/ZM3M->
363 [YNJ](https://doi.org/10.25493/ZM3M-YNJ)
- 364 49. E. R. Cullity, I.E. Bjerke, K. Kjelsberg, T. B. Leergaard, J. H. Kim (2020).
365 EBRAINS. <https://doi.org/10.25493/AVRZ-4JB>
- 366 50. T. B. Leergaard, J. G. Bjaalie, *Front. Neurosci.* **1**, 211 (2007).
- 367 51. R. Bakker, P. Tiesinga, R. Kötter, *Neuroinformatics* **13**, 353-366 (2015).
368



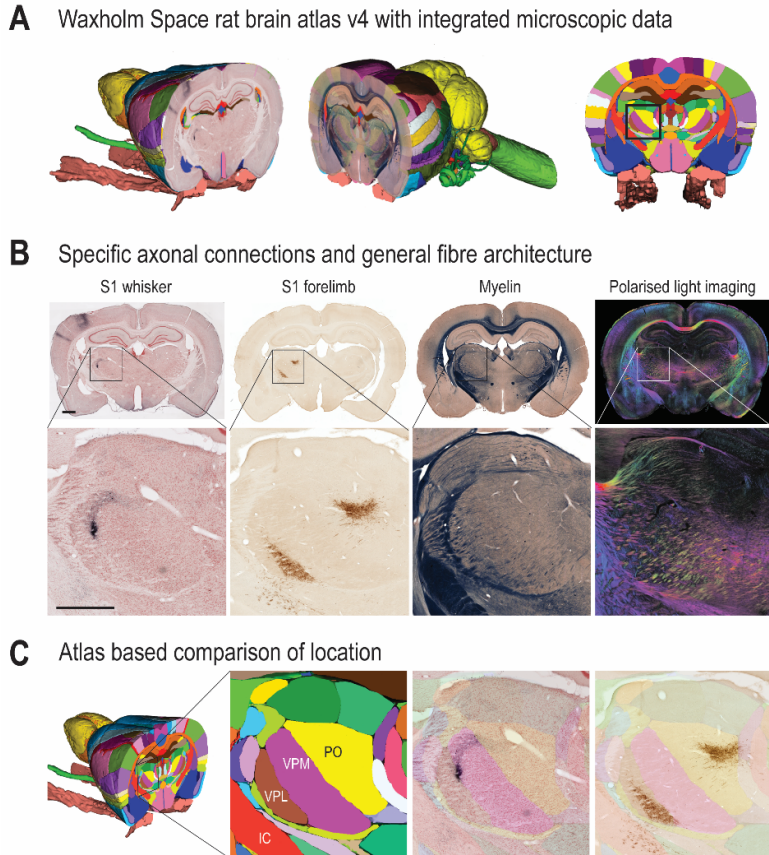
369

370 *Fig. 1. Wiring patterns in the brain*

371 **A,B**, Schematic visualizations of basal ganglia and cerebellar neural networks,
 372 topologically drawn (**A**) in an oblique slice through the Waxholm Space rat brain atlas
 373 (RRID: SCR_017124) and as a box diagram (**B**). **C**. Illustration of tract tracing
 374 experiments in which an anterograde tracer is placed in the cerebral cortex, taken up
 375 by groups of neurons, and transported along the axons and their branches, to visualize
 376 projections to intracortical and subcortical regions. (**D, E**) Microscopic images from a
 377 tract tracing experiment (data from 41), in which an axonal tracer (visualized as black
 378 labelling) was injected into the primary somatosensory cortex (**D**), giving anterograde
 379 labelling of dense axonal plexuses in thalamus (**E1**), caudoputamen (**E2**), and pontine
 380 nuclei (**E3**). CPu, caudoputamen; DCB, deep cerebellar nuclei; EPn, entopeduncular
 381 nucleus; GP, globus pallidus; SNc, substantia nigra, pars compacta; SNr, substantia
 382 nigra, pars reticulata; PN, pontine nuclei; PPN pedunculopontine nucleus; TN,
 383 trigeminal nuclei. Scale bars, 1 mm (**D**); 200 μ m (**E**).

384

385



386

387 *Fig. 2. Waxholm Space rat brain atlas with integrated microscopic data*

388 The Waxholm Space rat brain atlas is enriched with spatially registered microscopic
 389 image data allowing comparison across different experiments and data types. **(A)**

390 Illustration of tract tracing and myelin-stained microscopic images of coronal sections
 391 registered to the brain at the level of the thalamus, indicated with a frame. **(B)**

392 Overview and details from four different coronal microscopic images taken from the
 393 same anteroposterior level of the thalamus, including anterogradely labelled

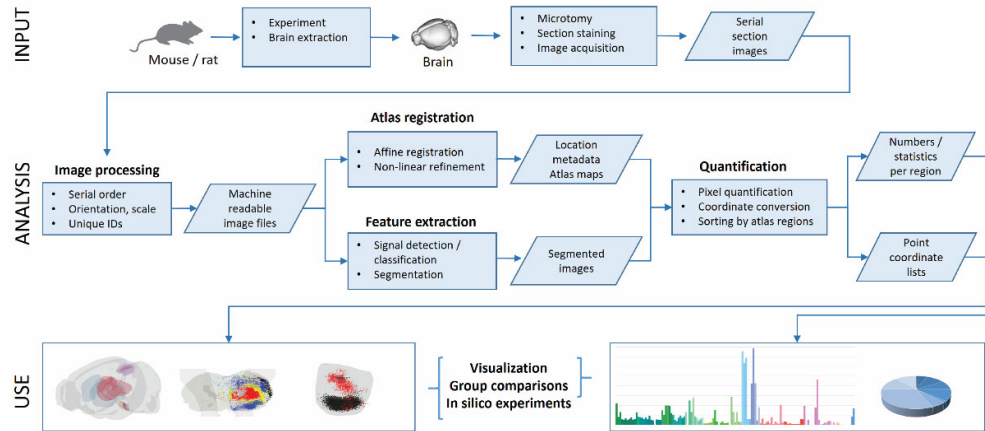
394 corticothalamic projections from whisker (data from 41) and forelimb (data from 42)
 395 representations in the primary somatosensory cortex (S1), tissue fibre orientations

396 visualized by myelin staining (data from 43), and polarized light imaging (data from
 397 44), respectively. **(C)** shows the Waxholm Space rat brain atlas superimposed on the

398 tract tracing image shown in B, providing a starting point for interpreting the spatial
 399 location of axonal labelling across subregions of the thalamus. Abbreviations: IC,

400 internal capsule; PO, posterior thalamic nucleus; VPL, ventral posterolateral thalamic
 401 nucleus; VPM, ventral posteromedial thalamic nucleus. Scale bars, 1 mm.

402



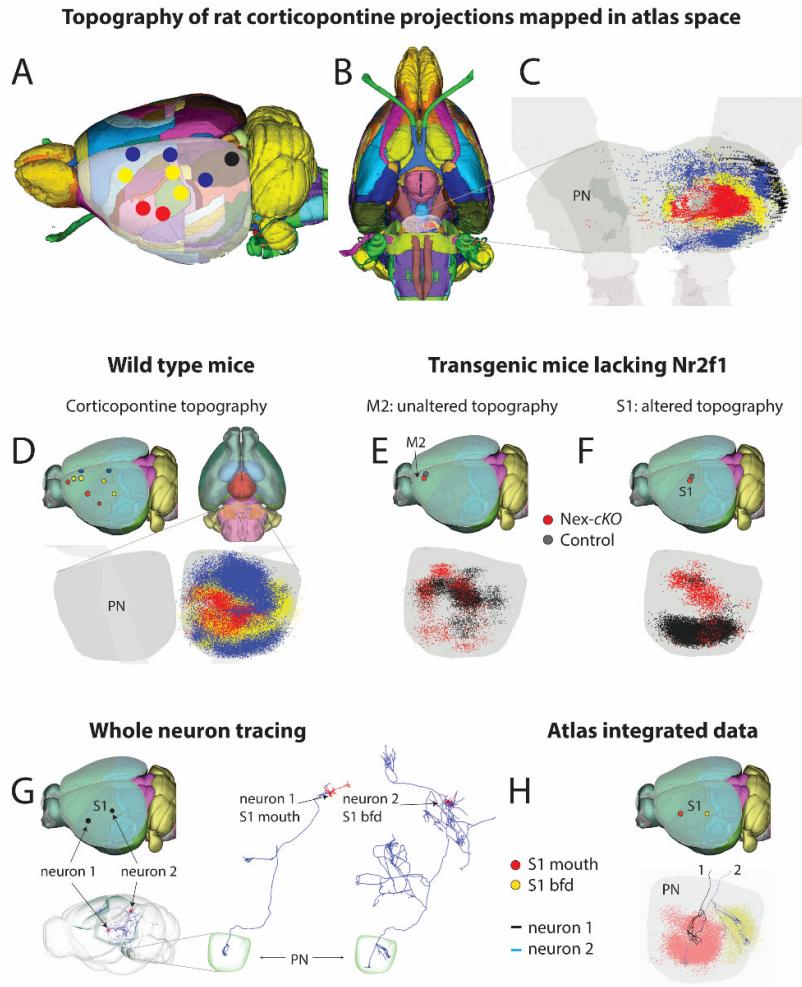
403

404 *Fig. 3. Workflow for data integration and atlas-based analysis*

405 Diagram showing key steps of a generic workflow for integration of rodent brain
 406 experimental data in volumetric brain reference atlases, and atlas based analysis,
 407 yielding quantitative data and 3-D point coordinate data sorted to atlas defined brain
 408 regions. The input to the workflow is provided by experimental procedures resulting
 409 in serial microscopic images of tissue sections showing neural labelling. Pre-
 410 processing steps include validation of image order and orientation, assignment of
 411 unique serial identifiers, to create machine readable image files. Important parallel
 412 analytic steps are the spatial registration of images to a volumetric reference atlas, and
 413 extraction of labelling signals from background, providing input combined in
 414 (automated) analyses extracting quantitative measures and 3-D point coordinates
 415 representing selected labelling features. The workflow output can be visualized and
 416 utilized in statistical analyses for characterizing and comparing labelled parameters.
 417 Point coordinates representing labelled neuronal elements are suitable for interactive
 418 3-D visualization and exploration of spatial distribution patterns, and hypothesis-
 419 driven *in silico* experiments visualizing selected combinations of data. Usage example
 420 data are taken from (45-49).

421

422



423

424 *Fig. 4. Three-dimensional analysis of spatially integrated connections data*

425 Examples illustrating studies of spatial organization in the first link of the rat and
 426 mouse cerebro-cerebellar circuit, based on tract-tracing data integrated and co-
 427 visualized in the Waxholm Space rat brain atlas (A-C) and the Allen Mouse Brain
 428 Common Coordinate Framework, CCFv3 (E-G). A-C, data combined from several rat
 429 brain experiments in which an axonal tracer was placed at separate locations in the
 430 cerebral cortex (A), and anterogradely labelled fibres were semiquantitatively
 431 represented as point coordinates spatially registered within the pontine nuclei. B
 432 shows the Waxholm Space rat brain atlas in view from ventral. C shows the outer
 433 boundaries of the pontine nuclei and descending corticofugal fibre tract as grey
 434 transparent surfaces, and data representing axonal labelling from different
 435 experiments as colour coded point clouds. Shifts in location of tracer injection sites
 436 from anterolateral to dorsomedial locations (A) corresponds to topographic shifts
 437 from internal to external lamellar subspaces in the pontine nuclei (C,). D-F, data

438 from a study of the impact of the cortical area-patterning gene *Nr2f1* on topographical
439 organization of corticopontine projections in mice, combining tract-tracing data from
440 the Allen Mouse Brain Connectivity Atlas with experimental data from transgenic
441 mice lacking cortical expression of *Nr2f1* (40). **D**, co-visualization of color-coded 3D
442 data points representing the distribution of corticopontine projections from different
443 cortical locations in wild-type mice show a similar inside-out topographical
444 organization as demonstrated in rats (50) (**A-C**). Comparison of the topographical
445 distribution of pontine projections arising from corresponding locations in the
446 secondary motor cortex (**E**), and primary somatosensory cortex (**F**) of *Nex-cKO*
447 transgenic mice lacking *Nr2f1* and control animals demonstrates that corticopontine
448 projections from the primary somatosensory cortex are altered in *Nex-cKO* mice, to
449 resemble the projections from the secondary motor cortex. **G-H** illustrate data from
450 different sources can be integrated and compared in atlas space. **G** shows whole brain
451 reconstructions of two projections neurons (from the Janelia Research Campus
452 MouseLight project, 21) located in the mouth and whisker representations of the
453 primary somatosensory cortex, with a variable amount of profusely branching axons
454 in several subcortical regions, including the pontine nuclei. **H** exemplifies a
455 comparison of corticopontine projections from single neurons and anterogradely
456 labelled projections from two populations of neurons in the mouth and whisker
457 representations in the primary somatosensory cortex (data derived from the Allen
458 Mouse Brain Connectivity Atlas, 5), indicating the trajectory of single cell projections
459 relative to the point cloud representing the spatial distribution of projections from a
460 larger amount of neurons in the same part of the cerebral cortex. The data shown in
461 **A-C** were taken from (46, cases R113-BDA, R118-BDA, R124-BDA; 47, cases D55-
462 FR; 48, cases M27-BDA, M27-FR; 49, cases R409-BDA, R412-BDA, R413-BDA).
463 The data shown in **E**, **F**, and **H** were taken from (40; wild type cases: 100141780,
464 112229814, 112952510, 126908007, 127084296, 127866392, 141602484,
465 141603190, 585025284; *Nex-cKO* cases: 11643_17, 19423_7; littermate control case:
466 18035_1). The neuron reconstructions shown in **G** were taken from the Janelia
467 MouseLight project (20, 21; <https://www.janelia.org/project-team/mouselight>; neuron
468 AA0945, <https://doi.org/10.25378/janelia.7804034> (#1), neuron AA1049;
469 <https://doi.org/10.25378/janelia.7822322> (#2)). Atlas surfaces and data points were
470 co-visualized using the MeshView web application, RRID: SCR_017222,
471 <http://www.nitrc.org>. Neuron reconstructions in **G** were visualized using the Scalable

472 Brain Atlas Composer (<https://sba-dev.incf.org/composer>; 51). Abbreviations: bfd,
473 barrel field; M2, secondary motor cortex; S1, primary somatosensory cortex, PN,
474 pontine nuclei.